Electronic Supplementary Material (ESI) for Physical Chemistry Chemical Physics.

Supplementary Information for

Accumulation and ordering of P3HT oligomers at the liquid-vapor interface with implications for thin-film morphology

Jakub K. Sowa, Thomas C. Allen, Peter J. Rossky

Peter J. Rossky, peter.rossky@rice.edu

This PDF file includes:

Supporting Information Text

1. Force field validation

The force field was constructed as described in the Methods section. For convenience, the topology files can be found at https://figshare.com/articles/dataset/Trajectory_and_topology_files_for_MD_simulations_of_P3HT/21817578

To validate the used force field, we performed simulations of the P3HT 16-mer in gas phase (30 ns in an NVT ensemble) and in a chlorobenzene solution (10 ns in an NPT ensemble at $T = 300$ K and $p = 1$ bar; Berendsen barostat (1) was used with $\tau_p = 2$ ps) and investigated the distribution of S-C-C-S dihedral angles. The resulting distributions are shown in Figure S1. We observe the maxima at around $\pm 145^\circ$ (the *trans* configuration) and around $\pm 40^\circ$ (the *cis* configuration). We also obtained the relative *cis:trans* ratios of approximately 1:4 and 1:10 for the bulk solution and gas phase simulations, respectively.

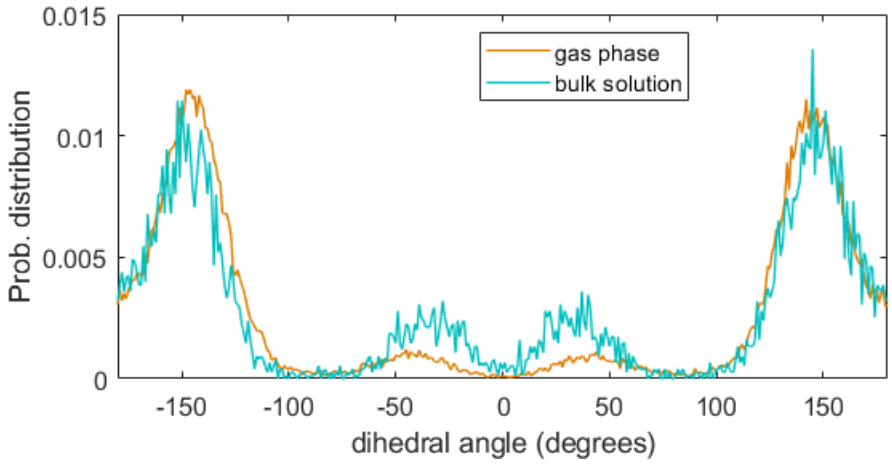

Fig. S1. Distribution of dihedral S-C-C-S angles in gas phase and in chlorobenzene solution.

The positions of the energy minima agree with those obtained using DFT by Khlaifia *et al.* (2) and Son et al. (3) as well as are consistent with the previous quantum-classical simulations of Simine and Rossky (4). We further find the *trans* geometry to be lower in energy, in agreement with the above calculations.

2. Slab geometries

The slab geometries are obtained as follows. We place the desired number of 16-mer chains (1 for the infinite dilution case, 10 for the 102 mg/mL simulation) in a simulation box which is then filled with chlorobenzene molecules (3000 and 2264 molecules, respectively). We perform an energy minimization, and NVT and NPT equilibrations in bulk. The z dimension of the sample space is then increased so that the height is at least three times larger than the thickness of the now slab-shaped solution. This is followed by another NVT equilibration. In the case of the highly concentrated solutions (with 2:1 and 1:1 chlorobenzene to 3HT ratios), we insert 200 16-mer chains together with the desired number (6400 or 3200) of chlorobenzene molecules into a box of $20 \times 20 \times 20$ nm and perform an NPT simulation until the size of the box stabilises. This is then followed by the same procedure as that just described.

3. Pulling simulations

Two umbrella sampling simulations were performed in this work; one at infinite dilution and one for a concentrated solution. The pulling coordinates in these simulations were the separation between the center of mass of an oligomer chain and the center of mass of the remaining slab; cosine weighting is used for the slab (5). We use the force constant of 1000 kJ/mol/nm^2 for the umbrella harmonic potential throughout. The set of geometries for the umbrella sampling were obtained by using as initial conditions a set of sequential positions obtained from a continuous pulling simulations performed at the rate of 0.001 nm/ps. We used 61 and 40 umbrella windows for the inifinite dilution and finite concentration cases, respectively. In the case of the infinite dilution, each of the geometries extracted from the pulling simulation was equilibrated for 11 ns and a run of 25 ns was used for calculating the PMF profile. In the finite concentration case, we used equilibration times of 20 ns and run times of 180 ns for each of the umbrella windows. The potential of mean force was obtained using the Weighted Histogram Analysis Method (WHAM) as implemented in GROMACS (6). The error estimates were obtained using bootstrapping trajectories based on umbrella histograms (6) with 200 bootstraps in both cases.

4. Oligomer distribution at infinite dilution

As discussed in the main body of this work, in order to additionally verify the lack of a potential minimum near the interface at infinite dilution, we have performed additional simulations of the 16-mer in the chlorobenzene slab. We used the same initial

geometries but generated new initial velocities for each case. We performed 3 runs and investigated the distributions of the center of mass of the oligomer. The center of mass trajectories and symmetrised distributions of the centers of mass with respect to the center of the slab are shown in Figure S2.

As discussed in the manuscript, the oligomer is not drawn to the interface and thus there is no evidence for a potential minimum near the liquid surface.

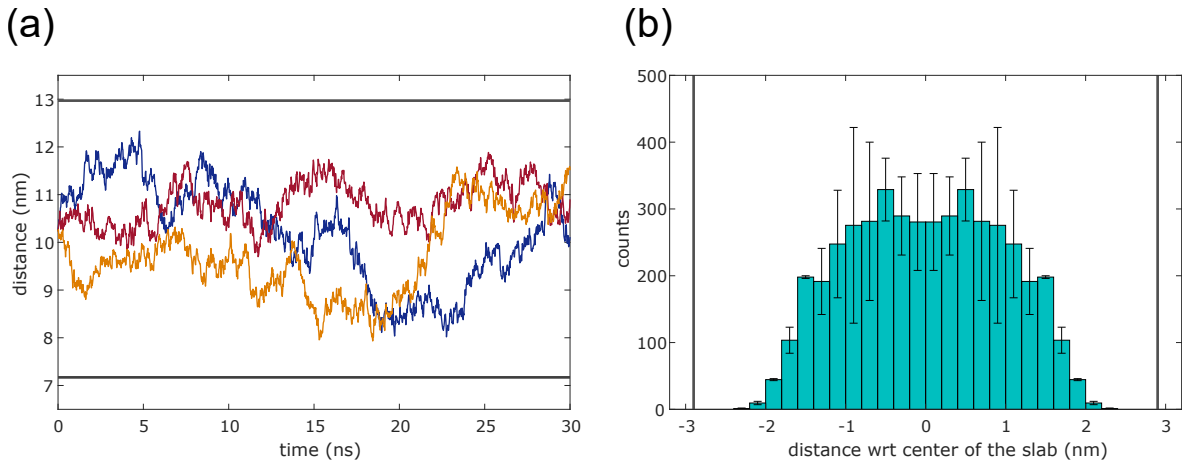

Fig. S2. (a) Trajectories for the centers of mass of the oligomers in three independent simulations. (b) Symmetrised distributions for the center of mass as a function of the z coordinate. Error bars denote the lower/upper values obtained at a given distance from the center of the slab. In both frames, gray solid lines indicate approximate positions of the liquid-vapor interfaces.

5. Oligomer geometries - further analysis

Firstly, for convenience, the histograms shown in Figures 2(C, D) are displayed here in a tabulated form in Figures S3 and S4.

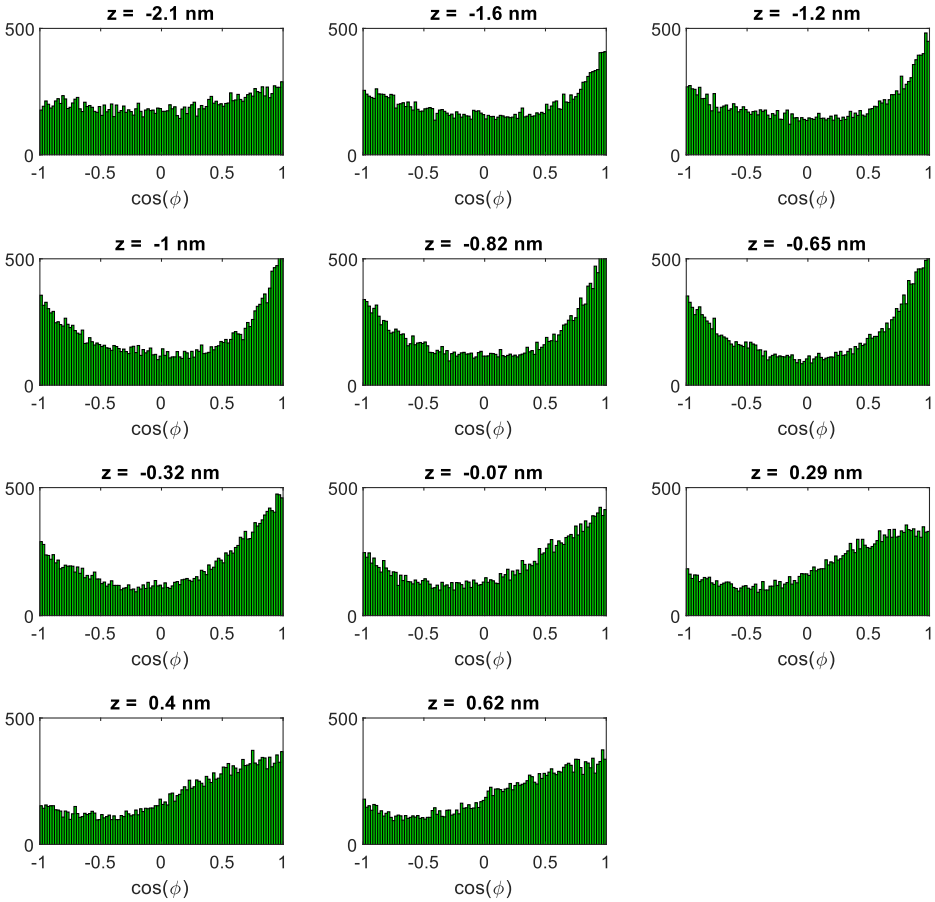

Fig. S3. Histograms showing the distributions of $\cos(\phi)$ (the angle between the hexyl vector and the surface normal) for various distances between the oligomer center of mass and the liquid-vapor interface.

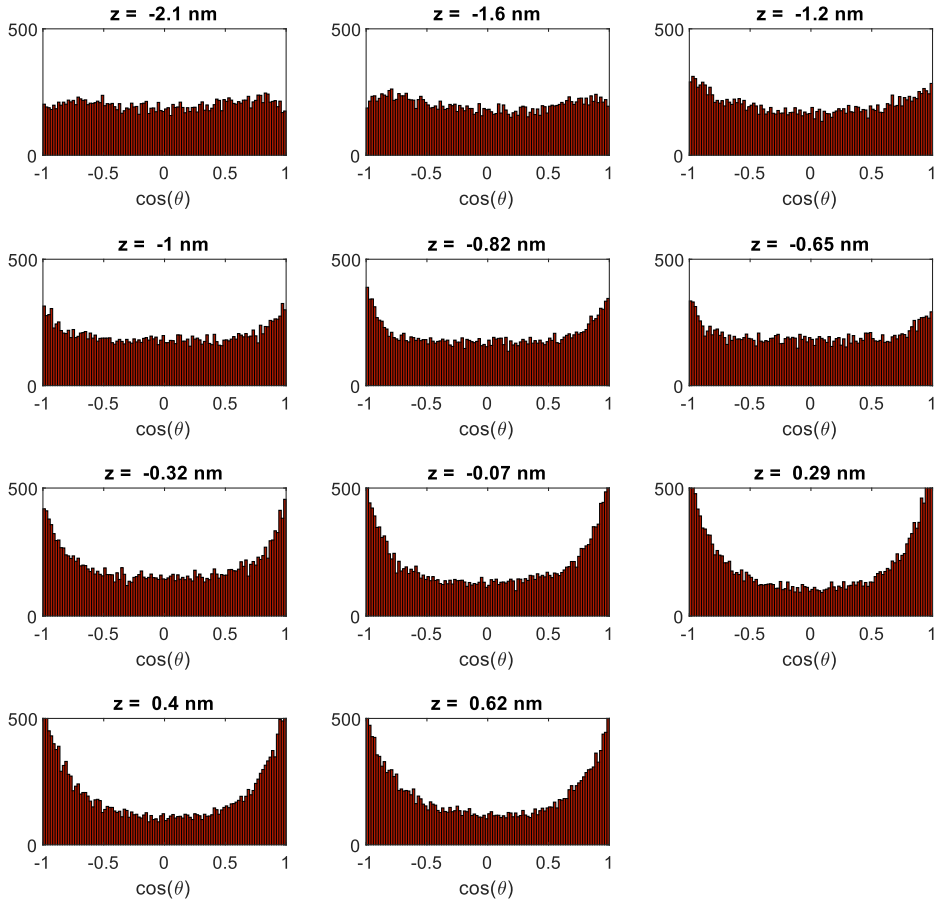

Fig. S4. Histograms showing the distributions of $\cos(\theta)$ (the angle between the thiophene ring vector and the surface normal) for various distances between the oligomer center of mass and the liquid-vapor interface.

Secondly, as discussed in the main body of this work, we analyze the propensity of the thiophene rings to align in the plane by fitting a $[\cos(\theta)+1]/2$ distributions to a beta distribution (7) which was chosen empirically solely based on the shape of the $\cos(\theta)$ histograms. The fitting procedure yields α and β, the two parameters of the beta distribution. In Figure S5(a), we plot the average value of these two parameters as well as the difference between them (off-set by 0.75 for clarity). Smaller values of α and β indicate a greater propensity of the thiophene rings for alignment parallel to the L/V interface. We can see that this tendency increases as the oligomer center of mass approaches the interface and plateaus past the linterface. The difference $(\alpha-\beta)$ indicates the asymmetry of the distribution. We can see that the distributions remain relatively symmetric. Figure S5(b) shows the high correlation between $(\alpha+\beta)/2$ and $\langle\cos(\phi)\rangle$.

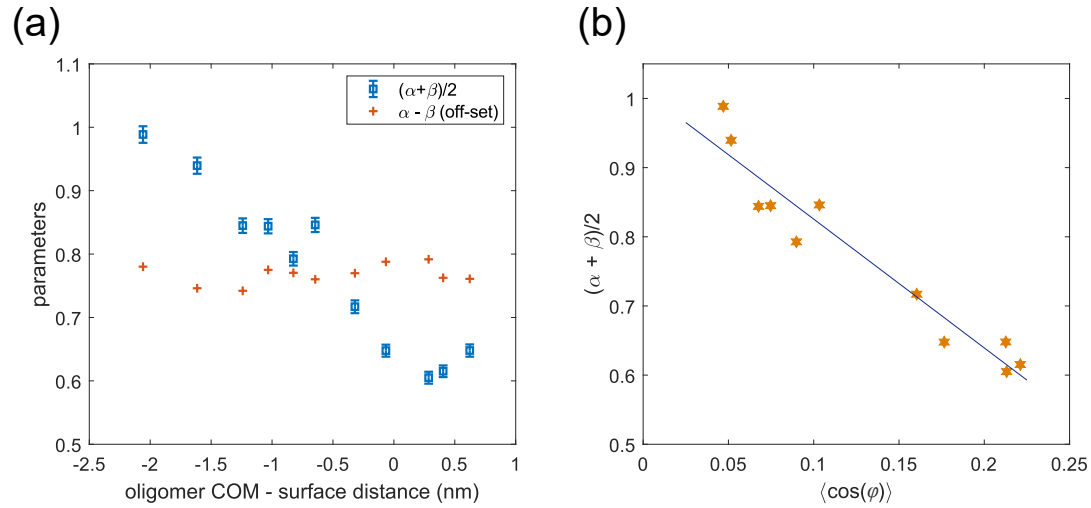

Fig. S5. (a) Extracted α and β parameters from the fits of the $\cos(\theta)$ histograms to a beta distribution. (b) Correlation plot between the values of $(\alpha+\beta)/2$ and $\langle\cos(\phi)\rangle$.

6. 102 mg/mL simulation

As discussed in the main body of the manuscript, we plot here the distribution of the oligomer centres of mass in the last 10 ns of the considered simulation. We also show the PMF profile evaluated using the symmetrized values of the COM distributions as $\mathrm{PMF}(z) = -k_\mathrm{B}T\ln[P(z)]$ where $P(z)$ is the distribution of the particle positions as a function of the z coordinate, normal to the surface of the slab.

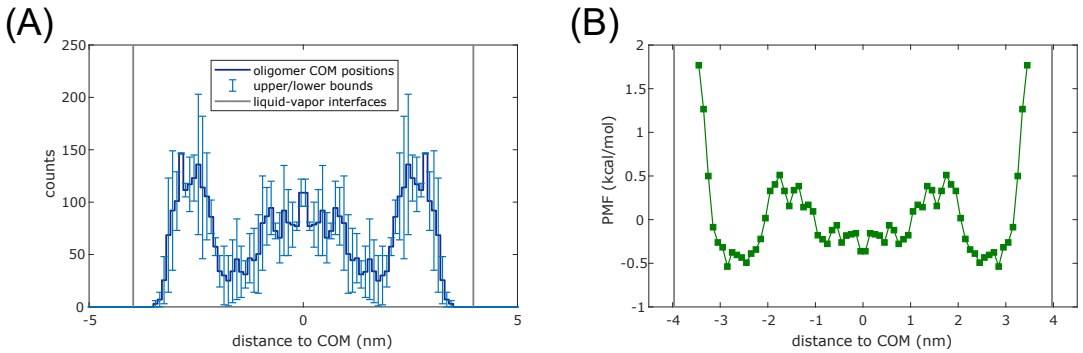

Fig. S6. (a) Histogram showing a (symmetrized) distribution of the centers of mass of the 10 oligomers during the final 10 ns of the nominally 100 mg/mL run. The error bars indicate the lower/upper values used for symmetrization. (b) The PMF profile obtained from distribution shown in (a). Also shown are the approximate positions of the two interfaces.

7. Toy model simulations

To additionally confirm that the accumulation of the oligomers near the liquid-vapor interface stems predominantly from the oligomer-oligomer interactions, we construct a simple toy model to evaluate the effects of such interactions.

A. Parametrization of the slab potential. First, we use the PMF profile obtained at infinite dilution to parametrize a force which will effectively create a 'slab' in the Langevin dynamics simulations. The derivative of the PMF profile is shown in Figure S7. We fit a 'bump' function defined as

$$F_i^{slab}(r_i) = A\exp\left(-\frac{p}{W+(r_i^z-z_0)^2}\right) \quad \text{if} \quad \left(z_0-\sqrt{W} < r_i^z < z_0+\sqrt{W}\right) \quad [1]$$

$$F_i^{slab}(r_i) = 0 \qquad \text{otherwise} \quad [2]$$

to the derivative of the potential of the mean force up to the distance of 5 nm. The resulting fit is also shown in Figure S7. We obtain $A = 143.5$ kcal/mol, $p = 6.52$ nm^2. $z_0 = 3.86$ nm, and $W = 4.9$ nm^2. We note that the interface in these simulations is located at $z \approx 2.86$ nm from the center of the slab (so that z_0 is found 1 nm above the interface).

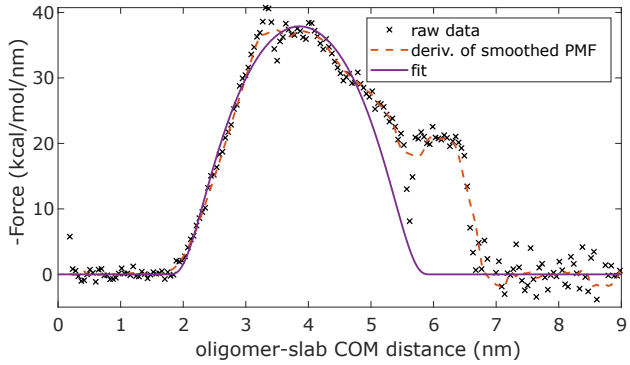

Fig. S7. The derivative of the (raw and smoothed) PMF profile and the fit to a 'bump' function profile.

B. Langevin dynamics. As discussed, the oligomers are modelled as particles, with positions r_i and velocities v_i, obeying the Langevin equation of motion (8), where $\mathrm{d}r_i/\mathrm{d}t = v_i$, and

$$m\frac{\mathrm{d}v_i(t)}{\mathrm{d}t} = -\lambda v_i(t) + \eta(t) + F_i(r) \quad [3]$$

where m is its mass, λ is the damping coefficient. $\eta(t)$ is the random force sampled from a Gaussian distribution with an average of zero, $\langle\eta(t)\rangle = 0$, and a correlation function $\langle\eta(t)\eta(t')\rangle = 2\lambda k_B T\delta(t-t')$. The final term describes the forces acting on the particles due to the particle-particle interactions as well as the force confining the particles within a slab, $F_i(r) = F_i^{inter}(r) + F_i^{slab}(r_i)$. The latter is (empirically) approximated following Eq. (1) at both slab interfaces. That is,

$$F_i^{slab}(r_i) = -A\exp\left(-\frac{p}{W+(r_i^z-z_0)^2}\right) \quad \text{if} \quad \left(z_0-\sqrt{W} < r_i^z < z_0+\sqrt{W}\right) \quad [4]$$

$$F_i^{slab}(r_i) = A\exp\left(-\frac{p}{W+(r_i^z+z_0)^2}\right) \quad \text{if} \quad \left(-z_0-\sqrt{W} < r_i^z < -z_0+\sqrt{W}\right) \quad [5]$$

and $F_i^{slab}(r_i) = 0$ otherwise, see below. This results in a slab in the x-y plane. The inter-particle force between two particles is given by $F_{inter}(r) = -\sum_{j\neq i}\mathrm{d}V_{ij}(r)/\mathrm{d}r$ where r is the distance between the two particles in question. We assume that the inter-particle potential has a Gaussian (soft-core) form (9, 10):

$$V_{ij}(r_{ij}) = \epsilon_0 \exp\left[-(r_{ij}/r_c)^2\right] \quad [6]$$

where r_{ij} is the distance between particles i and j, ϵ_0 determines the strength of the interaction, and r_c is the cut-off length.

We use physical parameters in our simulations. The mass of each particle is m = 2662.5 Da (which is the mass of a P3HT 16-mer) and the temperature is set to 300 K. The damping coefficient is estimated using the Stokes' law as $\lambda = 6\pi\mu R_g$, where μ is the viscosity of the liquid (using the value for chlorobenzene at 298 K, $\mu = 0.753$ mPa s) and R_g is the radius of gyration (estimated as $R_g \approx 1.70$ nm from our MD simulations in chlorobenzene). We note that the values of m and λ affect only the temporal dynamics and ought to have no effect on the equilibrium distribution of the particles in the slab. This gives rise to a slab of 7.32 nm thickness. Following the theory of Flory and Krigbaum (9), we set $r_c = 2R_g/\sqrt{3} \approx 1.96$ nm. The height of the potential is $\epsilon_0 = 2k_\mathrm{B}T$ (11).

The particles are randomly inserted into the slab, and their initial velocities are taken from the Maxwell-Boltzmann distribution. We use $N = 20$ particles and implement periodic boundary conditions in x and y. We also use an interaction cut-off of 5 nm. The width of the slab is fixed, and the effective concentration is controlled by varying the size of the unit cell in the x and y dimension; $L_x = L_y = L$ throughout. The Langevin dynamics is solved using the 'BAOAB' splitting method of Leimkuhler and Matthews (12). The simulations are run for 0.5 μs with a time step of 500 fs. We consider the concentrations of 1, 10, and 100 mg/mL which are obtained by setting $L = 109.9, 34.75$, and 11 nm, respectively.

C. Simulation results. In Figure S8(a), we plot the probability distributions for finding the particles within the slab as a function of their concentration and, in Figure S8(b), we show the corresponding potentials of mean force: $\mathrm{PMF}(z) = -k_\mathrm{B}T \ln[P(z)]$ where $P(z)$ is the distribution of the particle positions as a function of the z coordinate (normal to the surface of the slab).

At lower concentrations, the particles are almost uniformly distributed within the slab, in agreement with the infinite-dilution MD simulations. As the concentration of the particles increases, and at the point when it is comparable with the concentration used in Figure 3, we observe an accumulation of particles near the two interfaces. This particle distribution is adopted as it minimizes the overall effective repulsion between the particles. Our toy model reproduces the accumulation of oligomers in the vicinity of the interfaces. It predicts the minimum of the potential of the mean force to be situated around 0.9 nm below the interface in agreement with the MD simulations. Similarly, the depth of the potential (at around 0.5 kcal/mol) agrees with the results of MD simulations.

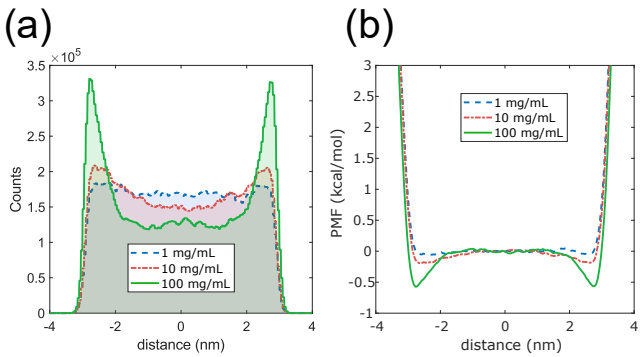

Fig. S8. Results from the toy-model Langevin dynamics. (a) Distribution of the particle positions at different concentrations. (b) Corresponding potential of mean force profiles relative to the center of the slab.

8. 1:1 slab - additional results

As discussed in the main body of this work, in Figure S9 below we show the top-down projection on the output geometry after 650 ns of relaxation. Shown are S, C2, and C3 atoms within 2 nm of the top interface.

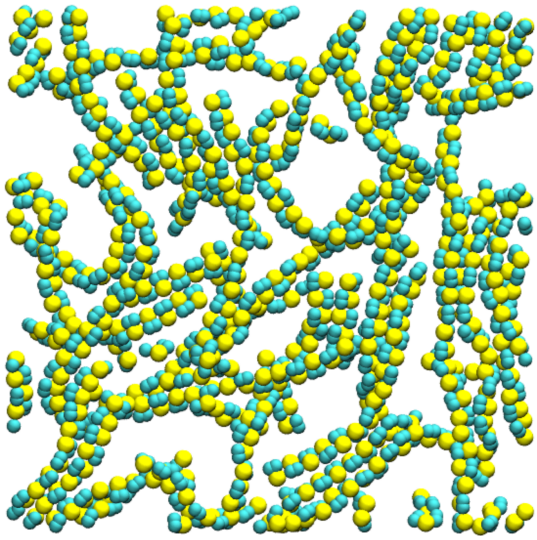

Fig. S9. Projection of the output geometry at the end of the production run at the top interface for the 1:1 slab. Shown are the S, C2, and C3 atoms (see Figure 7) within 2 nm of the top interface.

9. Results for the 2:1 slab

We first show a projected view of the oligomer chains located at the bottom and top interfaces; see Figure S10. We observe little evidence of ring-ring stacking.

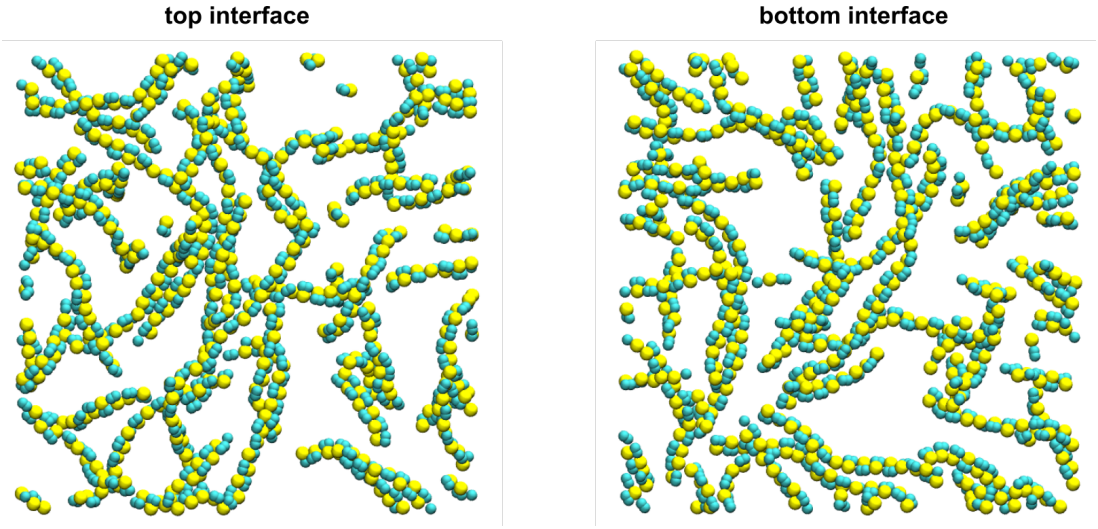

Fig. S10. Projection of the interfacial geometry (after 850 ns of relaxation) at the end of the production run for the 2:1 slab. Shown are the S, C2, and C3 atoms (see Figure 7) within 2 nm of the top and bottom L/V interface.

Next, in Figure S11, we plot the hexyl order parameter $P_2(t)$ and the distributions of the sulfur and the terminal hexyl carbon atoms during (the latter during the 550 ns following the 300 ns of relaxation), *c.f.* Figure 4 in the main text. We observe a lower $P_2(t)$ order parameter than at the interfaces of the more concentrated (1:1) slab but we can again see a clear accumulation of oligomers near the interfaces of the slab.

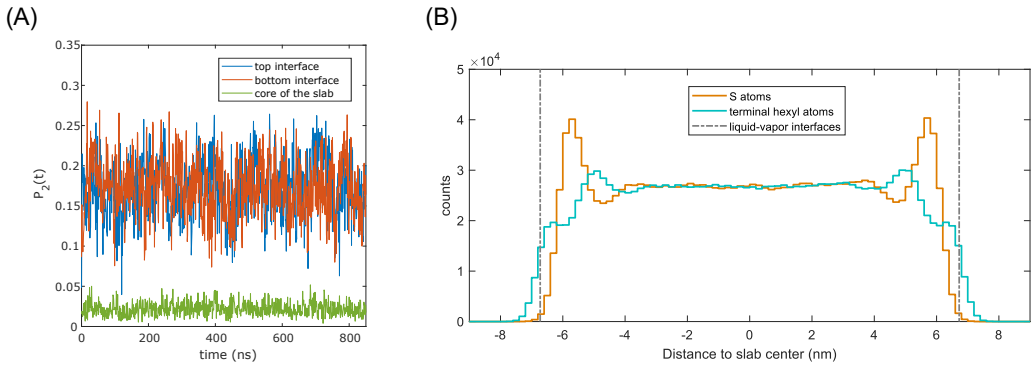

Fig. S11. (A) The hexyl order parameter $P_2(t)$ (see text) as a function of time for the two liquid-vapor interfaces and for a slice inside of the slab. (B) Distributions (unsymmetrized) of the sulfur atoms and the terminal hexyl carbon atoms over the course of the production run (550 ns following the 300 ns of relaxation). Compare to Figure 4 in the main text.

As discussed in the main text, Figure S12 compares the distributions of the angles between the thiophene and hexyl vectors and the normal to the interface at the two considered concentrations (that is, the 2:1 and 1:1 slab). As discussed in the main text, at the lower concentration, the thiophene rings preferentially align parallel to the interfaces in contrast to what can be observed for the 1:1 slab.

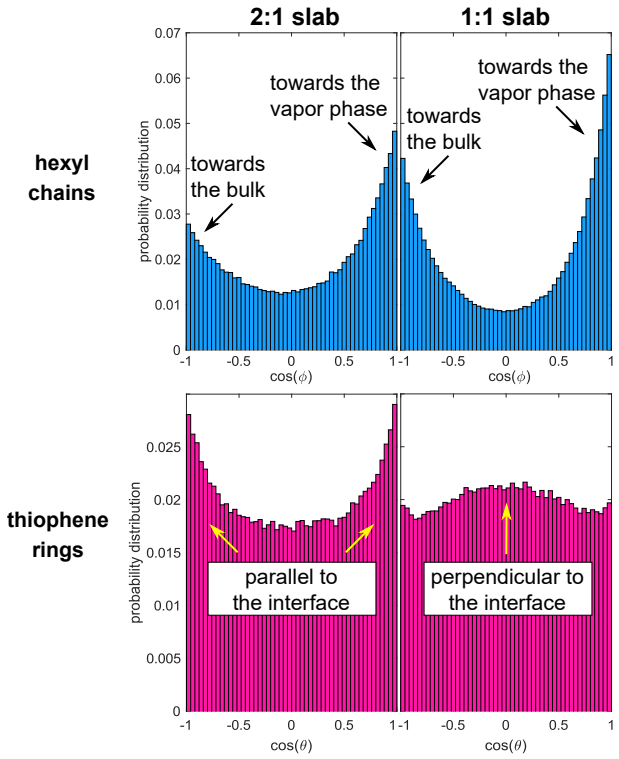

Fig. S12. Distributions of the angles between the hexyl and the ring vectors and the z-axis (normal to the surface of the slab) for the 2:1 and the 1:1 slab (provided the relevant ring center is found within 1.5 nm of the interface). Data is combined from the two interfaces. For a fair comparison, in both cases, data was taken from 350 ns production runs which followed 300 ns relaxations.

10. Radial density function

The radial density function, $\rho(r)$, is calculated by first identifying thiophene rings in the region of interest. For each ring, we then count and bin the number of thiophene rings (found in the given part of the system) at each distance r. We then average these distributions over the course of the production run and over all of the rings yielding a function $N(r)$. Finally, due to the pseudo-two dimensional character of this problem, we obtain the radial density function by considering $\rho(r) = N(r)/2\pi r$.

For the analysis of ring stacking, we begin by identifying thiophene rings within the relevant part of the slab. As inferred from the radial density function, we consider two rings to be stacked when their centres are within $r_0 = 0.6$ nm of each other (provided they are located on different oligomers). The relevant parameter, $|\cos(\kappa)|$, is the absolute value of the cosine of the angle between the relevant ring vectors, $\vec{r}_{ring}^{\,(i)}$ and $\vec{r}_{ring}^{\,(j)}$, which are defined in the Methods section.

11. Results for a chloroform slab

We performed analogous simulations for a slab of a solution of P3HT in chloroform (the chloroform force field was once again obtained using the LigParGen tool) (13).

We again considered a highly concentrated solution with a chloroform:3HT ratio of 2:1. We used a set of 100 P3HT 16-mers with 3200 chloroform molecules. The system was prepared analogously to what was described above. The simulation was run in an NVT ensemble for the total of 200 ns. Analogously to what we have done in the main body of this work, to facilitate faster equilibration, the simulation was performed at 353 K.

In Figure S13 we show the distribution of the sulfur atoms during the final 50 ns of the simulation together with (a) the density profile of the slab during this time, and (b) distribution of the terminal aliphatic (C10) atoms. We observe a clear accumulation of P3HT near the two interfaces analogous to what happens in the case of a chlorobenzene solution. As discussed in the manuscript, we also observe that the outer-most layer of the film consists primarily of the hexyl chains.

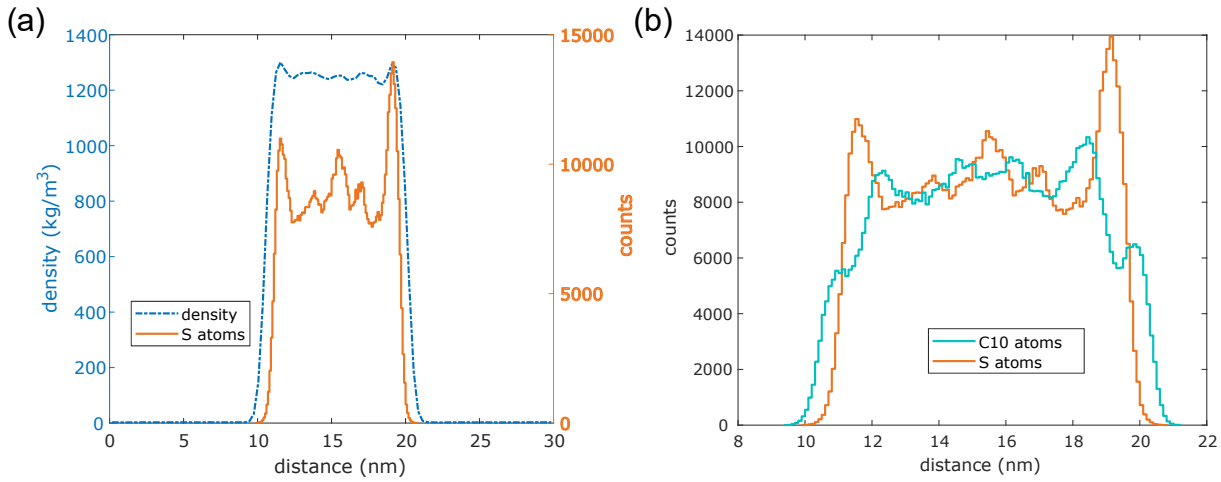

Fig. S13. Distributions of the sulfur atom positions during a 50 ns production run (which was proceeded by a 150 ns equilibration) together with (a) the average slab density during the production run, and (b) the distribution of the terminal hexyl carbon atoms.

12. Increased-polarity solvent

As discussed in the main body of this work, to demonstrate how the effects discussed here can be controlled by the properties of the solvent, we performed a slab simulation in which we doubled the partial charges on the chlorobenzene molecules thus increasing the solvent polarity. Using the same initial geometry as for the other 2:1 slab simulation, we performed a 600 ns relaxation simulation. Figure S14 shows the accumulation of the and alignment of oligomer chains in the vicinity of the interface (*c.f.* Figure 4 in the main text). In Figure S15, we show that the increase in concentration of oligomers near the interface also resulted in a large degree of stacking with evidence for up to 7 thiophene layers. Note that all of the features and trends observed here correspond to those found with the original solvent model, but they are notably amplified here.

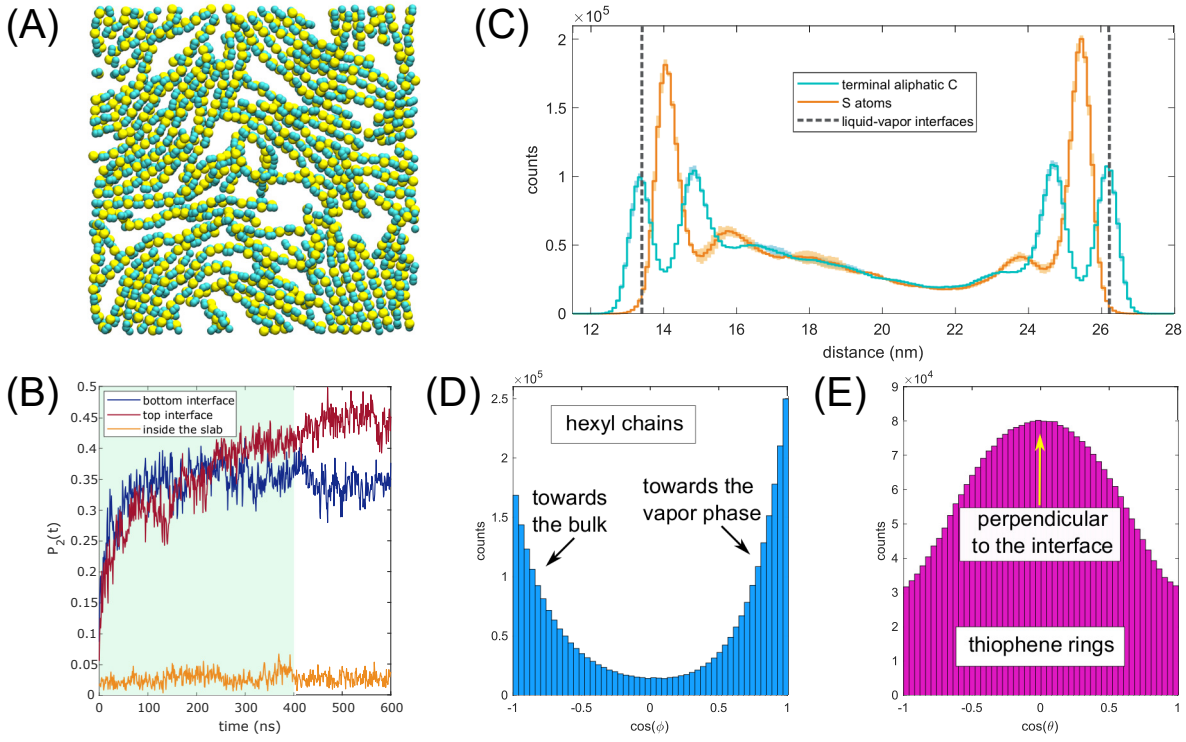

Fig. S14. Results from the simulations of the 2:1 slab with fictitiously polar solvent. (A) Top-down projection on the output geometry at the end of the production run (600 ns). Shown are the S, C2, and C3 atoms within 1.5 nm of the "top" interface. (B) The hexyl order parameter $P_2(t)$ (see text) as a function of time for the two L/V interfaces and for a slice inside of the slab. (C) Distributions (unsymmetrized) of the sulfur atoms and the terminal hexyl carbon atoms over the course of the production run. The shading indicates standard deviation error obtained from 50 ns segments. (D, E) Distributions of the angles between (D) hexyl and (E) ring vectors and the vapor phase-pointing normal to the plane of the slab provided the relevant ring center is found within 1.5 nm of an L/V interface. For panels (C-E), the first 400 ns are discarded as relaxation [as indicated in panel (B)].

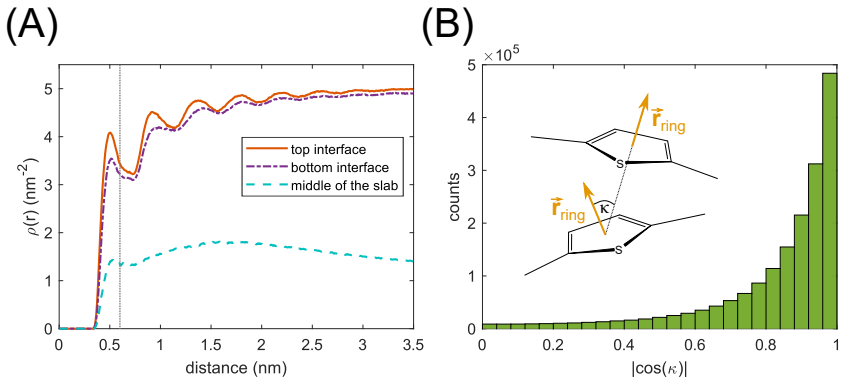

Fig. S15. (A) Radial distribution function for thiophene rings within 1.5 nm of the top/bottom interface and in a 1.5 nm region in the centre of the slab, calculated disregarding rings on the same chain. (B) Histogram of angles between neighbouring rings (see inset for definition) within 1.5 nm of the top interface. The first 400 ns is discarded as relaxation.

References

1. HJ Berendsen, Jv Postma, WF van Gunsteren, A DiNola, JR Haak, Molecular dynamics with coupling to an external bath. *J. Chem. Phys.* **81**, 3684–3690 (1984).
2. D Khlaifia, et al., Unraveling the real structures of solution-based and surface-bound poly (3-hexylthiophene)(p3ht) oligomers: a combined theoretical and experimental study. *RSC advances* **6**, 56174–56182 (2016).
3. SY Son, et al., High-field-effect mobility of low-crystallinity conjugated polymers with localized aggregates. *J. Am. Chem. Soc.* **138**, 8096–8103 (2016).
4. L Simine, PJ Rossky, Relating chromophoric and structural disorder in conjugated polymers. *The journal physical chemistry letters* **8**, 1752–1756 (2017).
5. O Engin, A Villa, M Sayar, B Hess, Driving forces for adsorption of amphiphilic peptides to the air- water interface. *J. Phys. Chem. B* **114**, 11093–11101 (2010).
6. JS Hub, BL De Groot, D Van Der Spoel, g_wham – A Free Weighted Histogram Analysis Implementation Including Robust Error and Autocorrelation Estimates. *J. Chem. Theory Comput.* **6**, 3713–3720 (2010).
7. M Abramowitz, IA Stegun, *Handbook of mathematical functions with formulas, graphs, and mathematical tables.* (US Government printing office) Vol. 55, (1964).
8. R Zwanzig, *Nonequilibrium Statistical Mechanics.* (Oxford University Press), (2001).
9. P Flory, W Krigbaum, Statistical mechanics of dilute polymer solutions. II. *J. Chem. Phys.* **18**, 1086–1094 (1950).
10. CN Likos, Effective interactions in soft condensed matter physics. *Phys. Rep.* **348**, 267–439 (2001).
11. A Louis, P Bolhuis, J Hansen, E Meijer, Can polymer coils be modeled as “soft colloids”? *Phys. Rev. Lett.* **85**, 2522 (2000).
12. B Leimkuhler, C Matthews, Robust and efficient configurational molecular sampling via Langevin dynamics. *J. Chem. Phys.* **138**, 05B601_1 (2013).
13. LS Dodda, I Cabeza de Vaca, J Tirado-Rives, WL Jorgensen, Ligpargen web server: an automatic opls-aa parameter generator for organic ligands. *Nucleic acids research* **45**, W331–W336 (2017).